Quantum phase transition and critical behavior between the gapless topological phases

Hao-Long Zhang,[1,*] Han-Ze Li,[2,3,4,*] Sheng Yang,[5,†] and Xue-Jia Yu[1,‡]

[1]*Fujian Key Laboratory of Quantum Information and Quantum Optics, College of Physics and Information Engineering, Fuzhou University, Fuzhou, Fujian 350108, China*

[2]*Institute for Quantum Science and Technology, Shanghai University, Shanghai 200444, China*

[3]*Department of Physics, Shanghai University, Shanghai 200444, China*

[4]*School of Physics and Optoelectronics, Xiangtan University, Xiangtan 411105, China*

[5]*Institute for Advanced Study in Physics and School of Physics, Zhejiang University, Hangzhou 310058, China*

(Received 18 April 2024; accepted 10 June 2024; published 27 June 2024)

The phase transition between gapped topological phases represents a class of unconventional criticality beyond the Landau paradigm. However, recent research has shifted attention to topological phases without a bulk gap, where the phase transitions between them are still elusive. In this work, based on large-scale density-matrix renormalization-group techniques, we investigate the critical behaviors of the extended quantum XXZ model obtained by the Kennedy-Tasaki transformation. Using fidelity susceptibility as a diagnostic, we obtain a complete phase diagram, which includes both topological nontrivial and trivial gapless phases. Furthermore, as the XXZ-type anisotropy parameter Δ varies, both the critical points h_c and correlation length exponent ν remain the same as in the $\Delta = 0$ case, characterized by $c = 3/2$ (Ising plus free boson) conformal field theory. Our results indicate that fidelity susceptibility can effectively detect and reveal a stable unconventional critical line between the topologically distinct gapless phases for general Δ. This work serves as a valuable reference for further research on phase transitions within the gapless topological phase of matter.

DOI: 10.1103/PhysRevA.109.062226

I. INTRODUCTION

The classification of the quantum phase of matter constitutes a core issue in condensed-matter and statistical physics [1–4]. Nevertheless, in the past few decades, the development of topological phases has received significant attention [5–10], expanding our understanding of quantum phases beyond the Landau paradigm. A notable example is the symmetry-protected topological (SPT) phases [7–9], where the bulk is gapped and nontrivial gapless modes emerge at the boundary. It is worth emphasizing that discussions of SPT phases typically focus on gapped quantum phases [11–19]. Despite the crucial role of the bulk gap in defining topological phases, recent research [20–47] has revealed that many key features of topological physics, such as degenerate edge modes, persist in the gapless systems, even in the presence of nontrivial coupling between the boundary and critical bulk fluctuations, which we refer to as gapless topological phases. These new phases are not described by the Landau paradigm, and recent studies have explored their exotic properties [36,38–45,47]. However, the phase transitions between them remain largely unexplored.

On a different front, the development of the theory of quantum phase transitions (QPTs) stands as one of the striking achievements in modern physics [1,48,49]. The traditional theory of phase transitions relies on the Landau-Ginzburg-Wilson symmetry-breaking paradigm [50]. However, in the past few decades, it has become clear that this paradigm does not fully capture the complexities at quantum critical points (QCPs), which are referred to as unconventional QCPs [51–53]. A notable example is the topological phase transitions between the gapped topological phases, which cannot be described in terms of fluctuating local order parameters or symmetry breaking [54–57]. Nonetheless, as mentioned in the preceding paragraph, the gapless topological phases represent a new type of exotic quantum matter beyond the Landau paradigm, and their phase transitions may be highly nontrivial and worth exploring in depth [58–62].

Fidelity susceptibility is a concept borrowed from quantum information theory and has found widespread utility as a useful diagnostic for pinpointing QCPs in the realms of condensed-matter and statistical physics [63–75]. Its advantage lies in the fact that it does not require prior knowledge of order parameters or symmetry breaking. To date, fidelity susceptibility has proven effective in detecting various types of QCPs, including conventional symmetry-breaking QCPs [63,65], topological phase transitions [67], Anderson transitions [69], nonconformal commensurate-incommensurate transitions [70], deconfined quantum criticality [76], and even non-Hermitian critical points [71,77]. Nevertheless, it remains an open question whether fidelity susceptibility can detect quantum phase transitions between gapless topological phases and more importantly determine the critical exponents and universality class at these QCPs.

*These authors contributed equally to this work.

†Contact author: qamber_ys@zju.edu.cn

‡Contact author: xuejiayu@fzu.edu.cn

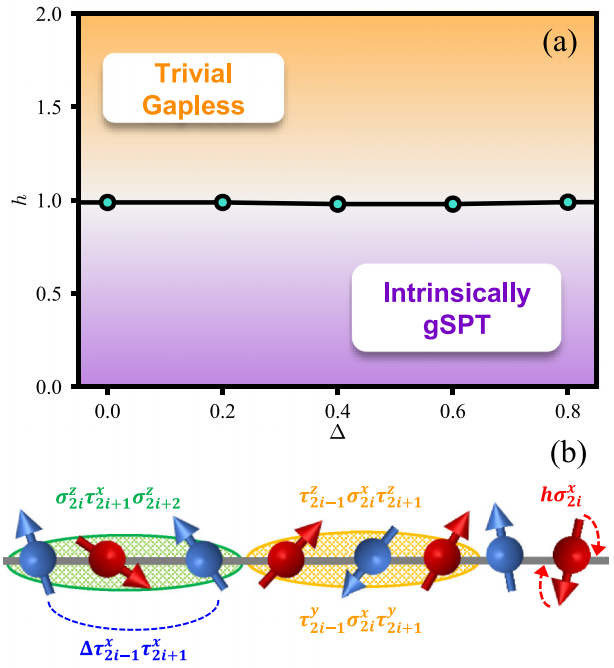

FIG. 1. (a) Phase diagram and (b) schematic representation of the extended quantum XXZ spin chain with the anisotropy parameter Δ and transverse field h. The critical point h_c^* is obtained from the polynomial fitting $h_c(N) = h_c^* + aN^{-1/\nu}$ of the peak position of fidelity susceptibility $h_c(N)$ for $N = 48, 56, 64, 72, 80, 88, 96$ sites. Symbols denote the numerical results of the critical values h_c^*.

In this work we take the first step towards addressing the above questions by investigating the QPT between trivial and intrinsically gapless symmetry-protected topological (gSPT) phases. We accomplish this by constructing a one-dimensional extended quantum XXZ spin model through the Kennedy-Tasaki (KT) transformation [41,78–80]. Specifically, using fidelity susceptibility as a diagnostic and in combination with the string order parameter and entanglement spectrum, we establish a complete global phase diagram, which includes both intrinsically gSPT and trivial gapless phases (see Fig. 1). Furthermore, by performing finite-size scaling on fidelity susceptibility, we conclude that as XXZ-type anisotropy parameters Δ vary, these topologically distinct gapless phases undergo a continuous phase transition, with the critical points h_c and correlation length exponent ν remaining the same as in the $\Delta = 0$ case, characterized by conformal field theory (CFT) with central charge $c = 3/2$ [46,81,82], which can be identified as an Ising CFT combined with a free boson CFT [41]. It indicates that the unconventional critical point between topologically distinct gapless phases for $\Delta = 0$ expands to a critical line for general Δ.

The paper is organized as follows. Section II contains the lattice model of the extended quantum XXZ spin chain after the KT transformation, the numerical method employed, the string order parameter, the entanglement spectrum, and the scaling relations of fidelity susceptibility. Section III shows the global phase diagram of the model and the finite-size scaling of the various physical quantities. A summary is presented in Sec. IV. Additional data for our numerical calculations are provided in the Appendixes.

II. MODEL AND METHOD

A. Extended quantum XXZ spin chain through the KT transformation

We consider a lattice model exhibiting topologically distinct gapless quantum phases. This model can be obtained by stacking an Ising-ordered Hamiltonian with an XXZ chain via the KT transformation [41]. The Hamiltonian is given by [38]

$$H = -\sum_{i=1}^{L} \left(\tau^z_{2i-1}\sigma^x_{2i}\tau^z_{2i+1} + \tau^y_{2i-1}\sigma^x_{2i}\tau^y_{2i+1} + \Delta\tau^x_{2i-1}\tau^x_{2i+1} + \sigma^z_{2i}\tau^x_{2i+1}\sigma^z_{2i+2} + h\sigma^x_{2i}\right), \quad (1)$$

where L denotes the number of unit cells, with the total number of sites N being twice that, i.e., $N = 2L$. Each unit cell is composed of a pair of spins $(\tau_{2i-1}, \sigma_{2i})$ represented by Pauli operators σ^α and τ^α on the even and odd sites, respectively. The parameter $h > 0$ acts only on even sites (σ spins) and denotes the strength of the transverse field. The XXZ-type anisotropic parameter Δ makes the Hamiltonian not exactly solvable in the sense of the Jordan-Wigner transformation. The system exhibits a class of gapless phases described by a $c = 1$ free boson CFT, possesses a $\mathbb{Z}_4$ symmetry generated by $U = \prod_i \sigma^x_{2i} e^{i(\pi/4)(1-\tau^x_{2i-1})}$, and also exhibits an emergent anomaly in the low-energy sector, known as intrinsically gSPT phases [34]. Specifically, in this sector, the $\mathbb{Z}_4$ symmetry is approximately realized as $U \sim \prod_i \sigma^x_{2i} e^{i(\pi/4)(1-\sigma^z_{2i-2}\sigma^z_{2i})}$, which is analogous to the anomaly observed on the boundary of a $(2+1)$-dimensional Levin-Gu SPT state [83]. This anomaly prevents the system from realizing a unique symmetry-preserving gapped phase and gives rise to interesting physical properties. Furthermore, in an open chain with a length N, the square of the low-energy symmetry operator fractionalizes onto each end of the boundary, as detailed in [44,45]. Specifically, $U^2 \sim \tau^x_1\sigma^z_2\sigma^z_{2L}$. This charge locally anticommutes with the U symmetry, protecting a twofold degeneracy in the intrinsically gSPT ground state.

In this work we solve the model using the density-matrix renormalization-group (DMRG) method [84–87] based on matrix product states (MPSs) [88–90]. The DMRG method stands as one of the most powerful unbiased numerical techniques for addressing one-dimensional strongly correlated many-body systems. We fix the maximal MPS bond dimension at 1024 to ensure reliable convergence of true energy eigenstates and fidelity susceptibilities (see Appendix E for details). To this end, we maintain relative energy errors below 10^{-9}. The fidelity susceptibility, defined later [Eq.(6)], is computed with a minimal step of $\delta h = 10^{-3}$. In practical DMRG calculations, a random initial state is chosen, and open boundary conditions are applied in most cases.

B. String order and entanglement spectrum in gapless topological phases

We first utilize the long-distance behavior of nonlocal string order parameters and the bulk entanglement spectrum under periodic boundary conditions (PBC) to identify the

possible quantum phases in the phase diagram before investigating QPT and pinpointing QCPs.

Following the KT transformation, as described in Ref. [41], the conventional local spin correlation function before the KT transformation is converted into string order parameters afterward, specifically denoted by σ and τ string correlations:

$$\mathcal{O}_\sigma(|i-j|) = \left\langle \sigma^z_{2i}\left(\prod_{k=i}^{j-1}\tau^x_{2k+1}\right)\sigma^z_{2j}\right\rangle, \tag{2}$$

$$\mathcal{O}_\tau(|i-j|) = \left\langle \tau^z_{2i-1}\left(\prod_{k=i}^{j-1}\sigma^x_{2k}\right)\tau^z_{2j-1}\right\rangle. \tag{3}$$

For $\Delta = 0.0$, in the trivial gapless phase ($1.0 < h < 2.0$), the σ string correlation exhibits exponential decay at long distances, while the τ string correlation function displays algebraic decay behavior. Conversely, in the intrinsically gSPT phase ($0.0 < h < 1.0$), the σ string correlation exhibits long-range order, while the τ string correlation still displays algebraic decay behavior.

Furthermore, the bulk entanglement spectrum encodes information beyond entanglement entropy, suggesting that the bulk ground-state wave function captures universal boundary information, such as topologically protected degenerate edge modes [91], and hence can be used to detect the gapped or gapless topological phases [38,92]. The entanglement spectrum consists of the eigenvalues of the entanglement Hamiltonian $\tilde{H}_A$, related to the reduced density matrix ρ_A of subsystem A by

$$\rho_A = \mathrm{Tr}_B|\Psi\rangle\langle\Psi| = \sum_\alpha e^{-\xi_\alpha}\left|\Psi^A_\alpha\right\rangle\left\langle\Psi^A_\alpha\right| = e^{-\tilde{H}_A}. \tag{4}$$

Here $|\Psi\rangle$ represents the ground-state wave function of the Hamiltonian and $\xi_\alpha \equiv -\ln\lambda_\alpha$, where λ_α is the eigenvalue of ρ_A. In our study of one-dimensional quantum chains, $A = 1, 2, \ldots, L/2$ and $B = L/2+1, \ldots, L$ represent a spatial bipartition of the entire chain, and the bulk entanglement spectrum displays two degenerate and nondegenerate ground states in topologically nontrivial and trivial gapless phases, respectively.

C. Fidelity susceptibility and scaling relations

In this work we utilize fidelity susceptibility, a concept borrowed from quantum information theory, offering a remarkably simple and intuitive method for identifying QCPs and obtaining critical exponents through finite-size scaling. The concept of fidelity susceptibility is as follows. Given a Hamiltonian $H(h) = H_0 + hH_1$ with a driving parameter h, the quantum ground-state fidelity $F(h, h+\delta h)$ is defined as the overlap amplitude of two ground states $|\psi(h)\rangle$ and $|\psi(h+\delta h)\rangle$:

$$F(h, h+\delta h) = |\langle\psi(h)|\psi(h+\delta h)\rangle|. \tag{5}$$

When a system undergoes a continuous phase transition from an ordered to a disordered phase by tuning the external field h to a critical value h_c^*, at which the structure of the ground-state wave function changes significantly, the quantum ground-state fidelity is nearly zero near h_c^*. In practice, a more convenient quantity for characterizing QPTs is the fidelity susceptibility, defined by the leading term of fidelity:

$$\chi_F(h) = \lim_{\delta h\to 0}\frac{2[1-F(h, h+\delta h)]}{(\delta h)^2}. \tag{6}$$

For a continuous QPT of a finite system with size N, fidelity susceptibility exhibits a peak at the pseudocritical point $h_c(N)$, and the true QCP h_c^* can be estimated through polynomial fitting $h_c(N) = h_c^* + aN^{-1/\nu}$ [93]. In the vicinity of $h_c(N)$, previous studies have shown that the finite-size-scaling behaviors of fidelity susceptibility $\chi_F(h)$ are described by [63]

$$\chi_F(h \to h_c(N)) \propto N^\mu, \tag{7}$$

where $\mu = 2 + 2z - 2\Delta_V$ is the critical adiabatic dimension. Here z is the dynamical exponent and Δ_V is the scaling dimension of the local interaction $V(x)$ at the critical point. On the other hand, it is shown that the fidelity susceptibility per site scales as [63]

$$N^{-d}\chi_F(h) = N^{(2/\nu)-d} f_{\chi_F}(N^{1/\nu}|h-h_c^*|), \tag{8}$$

where d is the spatial dimension of the system, f_{χ_F} is an unknown scaling function, and ν is the critical exponent of the correlation length, which can be easily computed according to the relation $\nu = 2/\mu$. Based on Eqs. (7) and (8), the values of critical exponents μ and ν can be determined and the corresponding critical behavior can be easily confirmed. In practice, the critical exponents ν and μ are usually extracted from fidelity susceptibility per site, $\chi_N(h) = \chi_F(h)/N^d$.

III. PHASE DIAGRAM AND CRITICAL BEHAVIOR

A. Quantum phase diagram: Overview

Before exploring phase transitions, let us investigate the possible quantum phases that appear in the phase diagram. In this work we focus only on $\Delta > 0$ since the $-\Delta$ case can be obtained through a π rotation around the x axis of every other τ spin, followed by the transformation $\Delta \to -\Delta$. As a first step, we examine a limiting case: When $\Delta = 0.0$, the model simplifies to an Ising-ordered Hamiltonian combined with an XY chain via the KT transformation. References [41,42] indicate that this model exhibits a phase transition between the intrinsically topological ($0.0 < h < 1.0$) and trivial gapless phases ($h > 1.0$). For a general Δ, since the model is no longer exactly solvable, we employ the DMRG simulations to ascertain the possible phases in the model by computing the scaling behavior of σ and τ string correlations for $\Delta = 0.2$ (see Appendix A for other Δ). As depicted in Figs. 2(a) and 2(b), we observed that when $h < 1.0$, σ and τ string correlations exhibit long-range order and power-law decay behavior, respectively, at the long-distance limit, consistent with the characteristics of intrinsically gSPT phases as we mentioned before. Conversely, when $h > 1.0$, σ and τ string correlations display exponential and power-law decay behaviors, respectively, consistent with the features of trivial gapless phases.

Furthermore, to elucidate the topological properties of gapless topological phases more clearly, we computed the bulk entanglement spectrum as a function of h under $\Delta = 0.2$ (see Appendix A for other Δ). As illustrated in Fig. 2(c), we observe that the ground-state degeneracy of the bulk entanglement spectrum transforms from twofold ($0.0 < h < 1.0$) to a unique ground state ($h > 1.0$). This indicates that the system

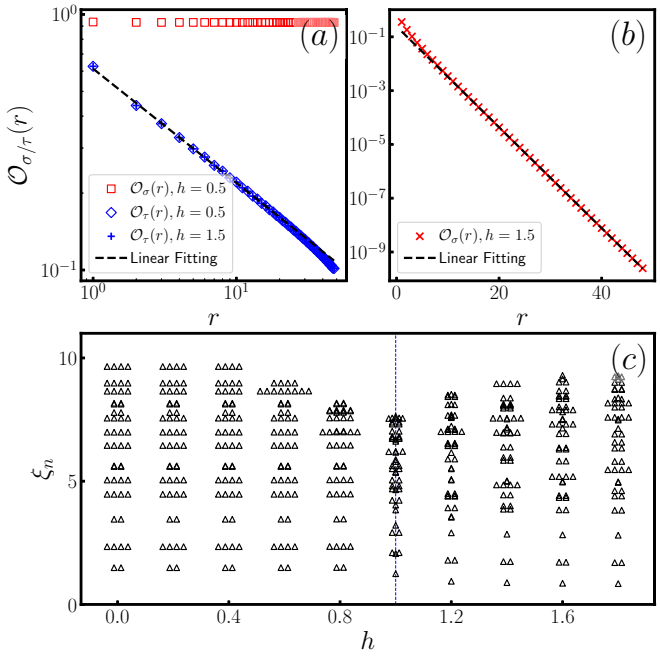

FIG. 2. Scaling behaviors of τ and σ string correlations in (a) the intrinsically gSPT phase ($h = 0.5$) and (b) the trivial gapless phase ($h = 1.5$) for $\Delta = 0.2$ and $N = 192$. (c) Evolution of the entanglement spectrum as a function of h for $\Delta = 0.2$ and $N = 96$ under PBC with only the first 50 low-lying values displayed in the plot.

undergoes a phase transition from a topologically nontrivial phase to a trivial gapless phase. Additionally, we notice that for $\Delta > 1.0$, the model exhibits a continuous phase transition between two distinct topologically trivial gapped phases at $h_c = 1.0$, characterized by a $(1 + 1)$-dimensional Ising universality class (see Appendix F for the details), which is not the focus of our paper.

The numerical results mentioned above suggest that irrespective of the magnitude of the XXZ-type perturbation, which breaks the integrability of the model, stable trivial and intrinsically gapless topological phases continue to exist in the ground-state phase diagram, determined through DMRG calculations for $N = 48, 56, 64, 72, 80, 88, 96$ sites, with the results presented in Fig. 1. When $\Delta = 0.0$, the ground state exhibits an intrinsically gSPT phase with a twofold degeneracy at $h \in (0.0, 1.0)$ and transitions to a trivial gapless phase as h becomes greater than 1.0, consistent with previous findings [41]. Additionally, for finite Δ, we find that the model exhibits a stable intrinsically gSPT phase and a trivial gapless phase across the entire range of Δ that we consider.

The finite-size-scaling behavior of fidelity susceptibility for $\Delta = 0.2$ with different N is presented in Fig. 3(a), which follows the scaling relation $\chi_N(h_c(N)) \propto N^{\mu-1}$ [Eq. (7)] near the second-order QPT critical point. As the system size N increases, the peak position $h_c(N)$ approaches the exact critical point value h_c^* more closely (see Appendix B for other Δ). Specifically, for the extended XXZ model with $\Delta = 0.2$, h_c^* is determined by the polynomial fitting $h_c(N) = h_c^* + aN^{-1/\nu}$ and then extrapolating to $N \to \infty$ [Fig. 3(b)]. According to Eq. (8), the fidelity susceptibility follows an exact scaling relation and collapses to one master curve [Fig. 4(b)],

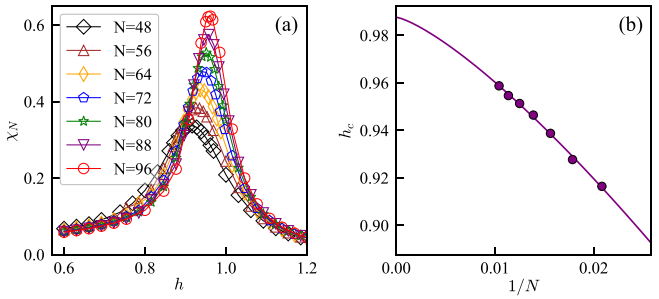

FIG. 3. (a) Fidelity susceptibility per site χ_F/N of the extended quantum XXZ spin chain for $\Delta = 0.2$ and $N = 48, 56, 64, 72, 80, 88, 96$ sites as a function of the transverse field h. Symbols denote the DMRG method results. (b) Extrapolation of the critical point h_c^* for different N. Symbols denote the finite-size DMRG method results for $\Delta = 0.2$ and $N = 48, 56, 64, 72, 80, 88, 96$ sites. We use the polynomial fitting $h_c(N) = h_c^* + aN^{-1/\nu}$ and extrapolate the critical point $h_c^* \approx 0.988(9)$.

confirming the appropriateness of the extrapolation. The finite-size-scaling behavior of fidelity susceptibility for other Δ values is also investigated (see Appendix C for details), and the results are presented in Table I. The findings indicate that the QCPs remain unchanged as Δ varies. This numerical observation can be understood by considering the model before the KT transformation, which is a quantum XXZ spin chain (τ spin) stacked with an Ising symmetry-breaking Hamiltonian (σ spin) with a transverse field acting on even sites. For $|\Delta| < 1.0$ and $0.0 < h < 2.0$, the ground state of the τ degree of freedom corresponds to gapless phases, while the ground state of the σ degree of freedom is in the symmetry-breaking phase for $h < h_c$ and in the trivial gapped phase for $h > h_c$. Since the anisotropy term Δ commutes with the KT transformation, after the KT transformation, the model exhibits topological and trivial gapless phases for $h < h_c$ and $h > h_c$, respectively. Therefore, since the tuning parameter only acts on even sites (σ spins), as long as $|\Delta| < 1.0$ (maintaining the τ degree of freedom as the gapless phase), the location of the critical point between the topological and trivial gapless phases remains unchanged.

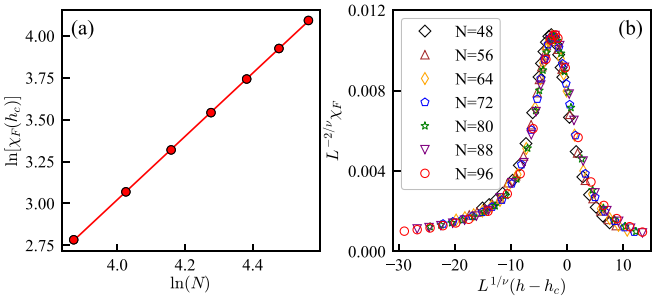

FIG. 4. (a) Finite-size scaling of the fidelity susceptibility per site $\chi_F(h_c)$ at the peak position h_c where $\mu \approx 1.894$. (b) Data collapse of fidelity susceptibility χ_F for the extended quantum XXZ spin chain. Symbols denote the finite-size DMRG method results for $\Delta = 0.2$ and $N = 48, 56, 64, 72, 80, 88, 96$ sites, where $\nu \approx 1.059(3)$, $\mu \approx 1.889(6)$, and $h_c^* \approx 0.988(9)$ are used for data collapse plots.

TABLE I. Critical exponents and critical points of the extended quantum XXZ chain for different Δ. The parentheses around the numbers represent the standard deviation of the least-squares fitting, accurate to the third decimal place.

Δ	h_c^*	μ	ν
0.0	0.988(9)	1.890(5)	1.058(3)
0.2	0.988(9)	1.889(6)	1.059(3)
0.4	0.979(4)	1.890(5)	1.058(2)
0.6	0.979(4)	1.890(4)	1.059(3)
0.8	0.99(1)	1.890(5)	1.058(2)
2.0	0.990(1)	1.890(5)	1.058(3)
3.0	0.980(3)	1.890(5)	1.058(3)

B. Finite-size scaling and critical exponents

The next questions concern the critical behavior of the extended XXZ chains with different Δ values and whether there exists a critical threshold Δ_c at which the critical behavior changes. To address these questions, we conduct large-scale DMRG simulations for various N in the region $0.0 \leqslant \Delta < 1.0$ to extrapolate the critical exponents μ and ν through the finite-size scaling of fidelity susceptibility.

The fidelity susceptibility per site, $\chi_N = \chi_F/N$, at the peak position $h_c(N)$ for different N at $\Delta = 0.2$ is illustrated in Fig. 4(a). The adiabatic critical dimension μ is well fitted by a polynomial function of $\chi_N(h_c(N)) = N^{\mu-1}(c + dL^{-1})$.

According to Eq. (8), the fidelity susceptibility can be scaled by $N^{-2/\nu}\chi_F$ as a function of $N^{1/\nu}(h - h_c^*)$ in the vicinity of the QCP h_c^*. The correlation length exponent ν is then determined by $\nu = 2/\mu$. By substituting the obtained critical point h_c^* and critical exponent ν into Eq. (7), all fidelity susceptibilities for different N collapse into a single curve [Fig. 4(b)], indicating the accuracy of the estimated critical point and critical exponent (see Appendix D for other Δ). It is worth noting that the peak in the data collapse is not precisely at 0 due to the finite-size effect for $h(N) = h_c^* + aL^{-1/\nu}$ ($a \neq 0$).

The extrapolations of the critical adiabatic dimension μ and the correlation length exponent ν for other Δ values are presented in Appendix C and the results for all Δ are summarized in Table I and Fig. 5. Both ν and μ remain unchanged as Δ varies. This indicates that the XXZ-type term acts as irrelevant perturbations and the unconventional critical point described by CFT with central charge $c = 3/2$ for $\Delta = 0.0$, as discussed in the literature [41], expands to a critical line for general Δ. This trend also suggests that the unconventional QCP between the topologically distinct gapless phases is robust against the XXZ-type perturbation. However, the anomalous dimension η is related to the Luttinger parameter and has been compared with the exact solution $\eta(\Delta) = 1 - \arccos(-\Delta)/\pi$, as shown in recent work [38] by some of the authors of the present paper. Therefore, the properties of the model are not fully characterized at $\Delta = 0$. Nevertheless, in this work, although the model exhibits the same correlation length exponents ν but distinct anomalous dimensions η for various values of Δ, we focus only on the universal features of the phase transition between the topologically distinct gapless phases, both characterized by Ising CFT combined with a free boson CFT.

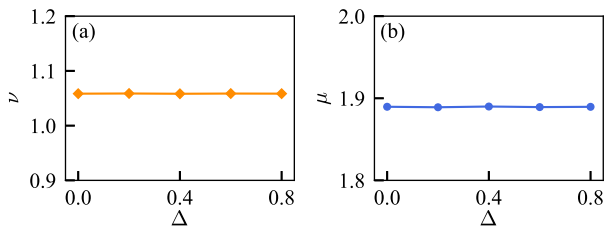

FIG. 5. (a) Correlation length exponent ν and (b) critical adiabatic dimension μ with respect to Δ. The symbols denote the finite-size DMRG method results that are obtained by extrapolating from the fidelity susceptibility $\chi_F(h_c(N))$ at the peak position $h_c(N)$ of $N = 48, 56, 64, 72, 80, 88, 96$ sites.

IV. CONCLUSION AND OUTLOOK

We have investigated the phase transition between topologically distinct gapless phases, namely, intrinsically gSPT phases. We established a complete phase diagram for the Hamiltonian, which is a one-dimensional extended XXZ model constructed by the KT transformation. Using fidelity susceptibility as a diagnostic and in combination with the string order parameter and entanglement spectrum, we unambiguously revealed the intrinsically gSPT and trivial gapless phases in the phase diagram. Moreover, by computing fidelity susceptibility and performing finite-size scaling, we observed a continuous phase transition between the topologically distinct gapless phases as the XXZ-type anisotropy term Δ varies. Remarkably, the critical points and correlation length exponent remain the same as in the $\Delta = 0$ case, characterized by CFT with central charge $c = 3/2$, which can be identified as an Ising CFT combined with a free boson CFT. Our results indicate that fidelity susceptibility can effectively detect and reveal an unconventional critical point for $\Delta = 0.0$ extended into a critical line for general Δ. Future intriguing questions involve exploring the critical behavior between topologically distinct gapless phases in higher dimensions and within different symmetry groups, e.g., $\mathbb{Z}_3$ and U(1), as well as constructing finite-temperature phase diagrams. Our work could shed new light on the phase transition between gapless topological phases of matter.

ACKNOWLEDGMENTS

We thank Linhao Li and Shao-Kai Jian for very helpful discussions. Numerical simulations were carried out with the ITENSOR package [94] on the Kirin No. 2 High Performance Cluster supported by the Institute for Fusion Theory and Simulation at Zhejiang University. X.-J.Y. acknowledges support from the start-up Grant No. 511317 of Fuzhou University.

APPENDIX A: STRING ORDER AND ENTANGLEMENT SPECTRUM FOR OTHER VALUES OF Δ

In this Appendix we provide additional data to identify the intrinsically gSPT and trivial gapless phases through the

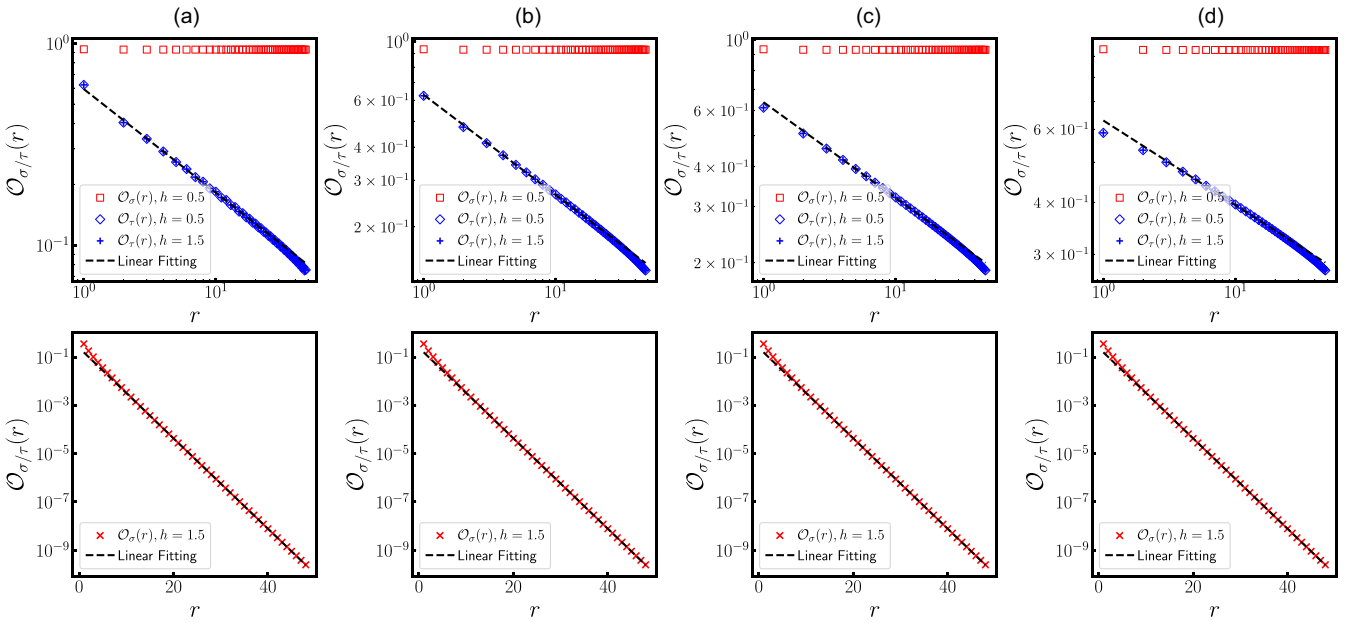

FIG. 6. Scaling behaviors of string correlations in the intrinsically gSPT phase ($h = 0.5$) and trivial gapless phase ($h = 1.5$) for (a) $\Delta = 0.0$, (b) $\Delta = 0.4$, (c) $\Delta = 0.6$, and (d) $\Delta = 0.8$. The simulated system size is $N = 192$ under OBC.

scaling behavior of string correlations and the entanglement spectrum for different Δ values.

On the one hand, as described in the main text, the long-distance behavior of the τ and σ string correlations can be completely different within the intrinsically gSPT and trivial gapless phases. Specifically, as shown in Fig. 6, we computed the τ and σ string correlations as a function of lattice distance r for $\Delta = 0.0$ [Fig. 6(a)], $\Delta = 0.4$ [Fig. 6(b)], $\Delta = 0.6$ [Fig. 6(c)], and $\Delta = 0.8$ [Fig. 6(d)] with a simulated system size of $N = 192$ under OBC. The results indicate that $h > 1$ and $h < 1$ exhibit the characteristics of trivial gapless and intrinsically gapless SPT phases, respectively.

On the other hand, to more intuitively exhibit the topological properties of gapless quantum phases, as in the main text, we calculated the bulk entanglement spectrum as a function of h under different Δ, i.e., $\Delta = 0.0$ [Fig. 7(a)], (b) $\Delta = 0.4$ [Fig. 7(b)], (c) $\Delta = 0.6$ [Fig. 7(c)], and (d) $\Delta = 0.8$ [Fig. 7(d)], with $N = 96$ under PBC. Here we display only the first 50 low-lying values in the plot. Our results indicate that regardless of the magnitude of Δ, the ground-state degeneracy of the entanglement spectrum changes from double degeneracy to a unique ground state at $h \approx 1.0$ (blue dashed lines in Fig. 7) as Δ increases. This change in topological properties is consistent with the change in the long-distance behavior of string correlations as mentioned in the preceding paragraph.

APPENDIX B: FIDELITY SUSCEPTIBILITY FOR OTHER VALUES OF Δ

In this Appendix we provide additional data to obtain the critical line via fidelity susceptibility for other values of Δ.

As in the main text, the fidelity susceptibility per site χ_N of the extended quantum XXZ spin chain for $\Delta = 0.0$ [Fig. 8(a)], $\Delta = 0.4$ [Fig. 8(b)], $\Delta = 0.6$ [Fig. 8(c)], and $\Delta = 0.8$ [Fig. 8(d)], with system sizes $N = 48, 56, 64, 72, 80, 88, 96$, is plotted as a function of the transverse field h in Fig. 8. We observe that, regardless of the value of Δ, the fidelity susceptibility exhibits obvious peaks as h varies, indicating continuous phase transitions between topologically distinct gapless phases. Moreover, we find that the QCPs remain unchanged for different values of XXZ-type perturbation.

APPENDIX C: QUANTUM CRITICAL POINT FITTING AND CRITICAL ADIABATIC DIMENSION FOR OTHER VALUES OF Δ

In this Appendix we provide additional data to extrapolate the accuracy of critical points and critical adiabatic dimensions for other values of Δ.

As in the main text, we determined the pseudocritical point $h_c(N)$ corresponding to the maximum values of the fidelity susceptibility and performed finite-size scaling of the pseudocritical point $h_c(N)$ as a function of inverse system sizes $1/N$ for $\Delta = 0.0$ [Fig. 9(a)], $\Delta = 0.4$ [Fig. 9(b)], $\Delta = 0.6$ [Fig. 9(c)], and $\Delta = 0.8$ [Fig. 9(d)], with $N = 48, 56, 64, 72, 80, 88, 96$ sites. The extrapolated critical points are summarized in Table I. The accurate critical point h_c^* remains unchanged with increasing Δ.

Furthermore, we examined the maximal fidelity susceptibility per site $\chi_N(h_c(N)) = \chi_F(h_c(N))/N$ as a function of system sizes N for $\Delta = 0.0$ [Fig. 10(a)], $\Delta = 0.4$ [Fig. 10(b)], $\Delta = 0.6$ [Fig. 10(c)], and $\Delta = 0.8$ [Fig. 10(d)], with $N = 48, 56, 64, 72, 80, 88, 96$ sites. The critical adiabatic dimensions are also summarized in Table I. We observe that the critical adiabatic dimension μ remains unchanged with increasing Δ.

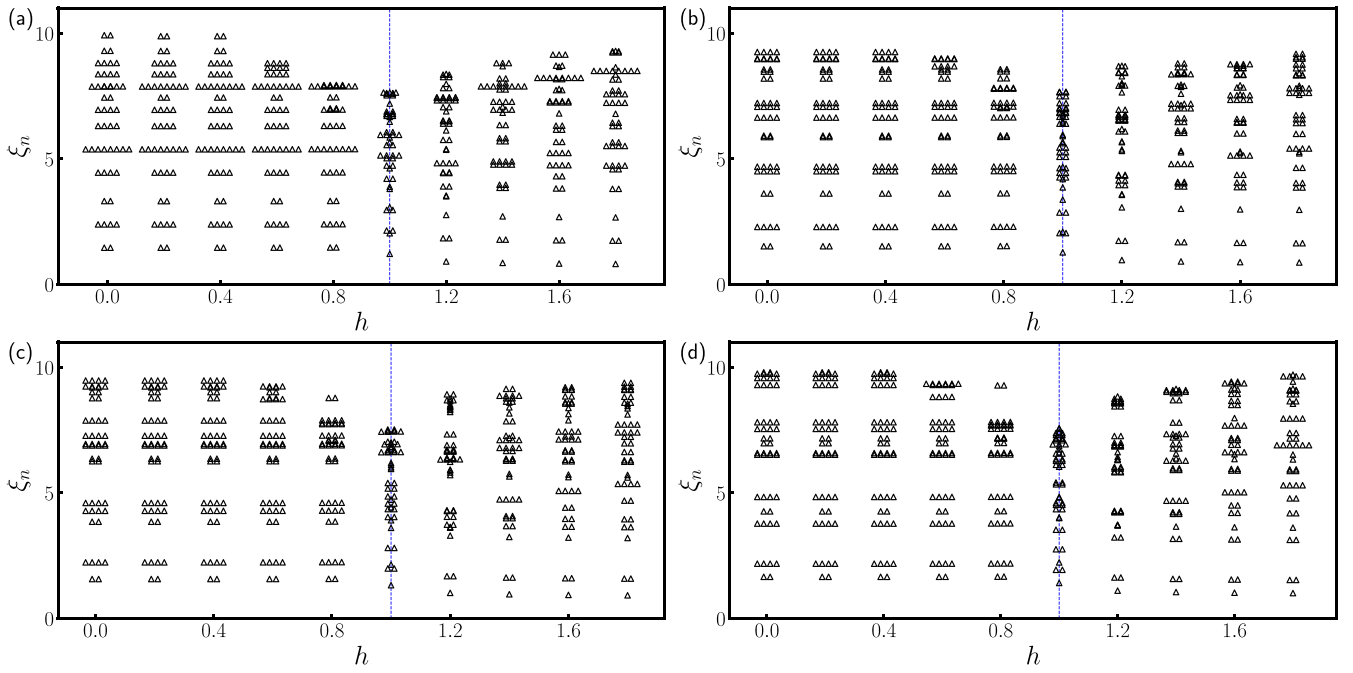

FIG. 7. Entanglement spectrum as a function of h for (a) $\Delta = 0.0$, (b) $\Delta = 0.4$, (c) $\Delta = 0.6$, and (d) $\Delta = 0.8$ with $N = 96$ under PBC. We display only the first 50 low-lying values in the plot.

APPENDIX D: DATA COLLAPSE FOR OTHER VALUES OF Δ

In this Appendix we present additional data demonstrating the variation in correlation length exponents ν of the extended quantum XXZ chain.

As in the main text, data collapse of fidelity susceptibility χ_F for the one-dimensional extended XXZ model is shown for $\Delta = 0.0$ [Fig. 11(a)], $\Delta = 0.4$ [Fig. 11(b)], $\Delta = 0.6$ [Fig. 11(c)], and $\Delta = 0.8$ [Fig. 11(d)], with $N = 48, 56, 64, 72, 80, 88, 96$ sites. The correlation length exponents are summarized in Table I. It is evident that the correlation length exponents of the extended quantum XXZ chain is the same as observed in the $\Delta = 0.0$ case, characterized by a CFT with central charge $c = 3/2$, which can be understood as a combination of Ising and free boson CFTs.

APPENDIX E: CONVERGENCE TESTING AND BENCHMARKING AGAINST EXACT DIAGONALIZATION FOR SMALL SYSTEM SIZES

In this Appendix we benchmark the performance of the DMRG method against exact diagonalization (based on the Lanczos algorithm) for small system sizes to validate the accuracy of the DMRG method.

Figure 12 shows the ground-state energy E_g and fidelity susceptibility χ_N for $\Delta = 0.4$ and $N = 24$ sites. As shown in Fig. 12(a), the ground-state energy E_g calculated by the DMRG method (blue circles) and exact diagonalization (red pluses) as a function of the external field h demonstrates close agreement, indicating the high accuracy of the DMRG method. As shown in Fig. 12(b), the fidelity susceptibility per site χ_N calculated by the DMRG method (blue circles) and exact diagonalization (red crosses) as a function of h

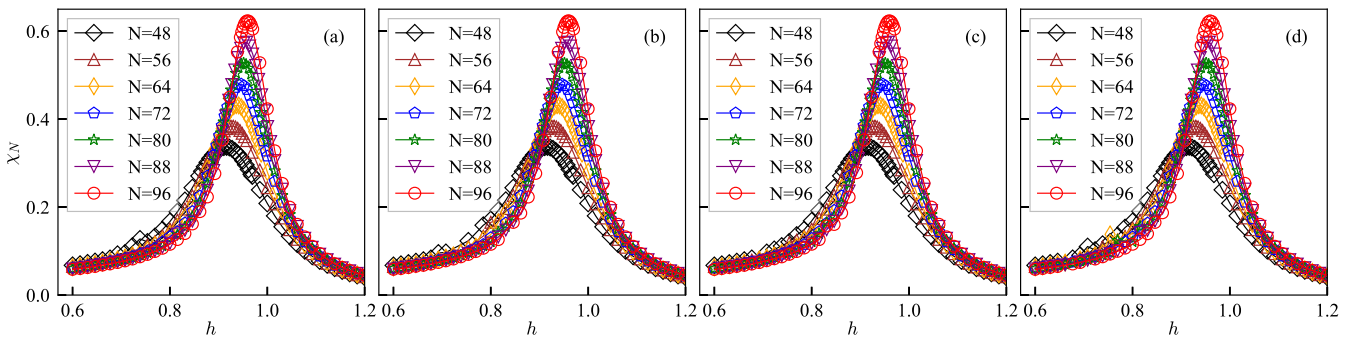

FIG. 8. Fidelity susceptibility per site χ_N for the extended quantum XXZ spin chain for (a) $\Delta = 0.0$, (b) $\Delta = 0.4$, (c) $\Delta = 0.6$, and (d) $\Delta = 0.8$ with $N = 48, 56, 64, 72, 80, 88, 96$ sites as a function of the driving parameter h. Symbols denote finite-size DMRG method results.

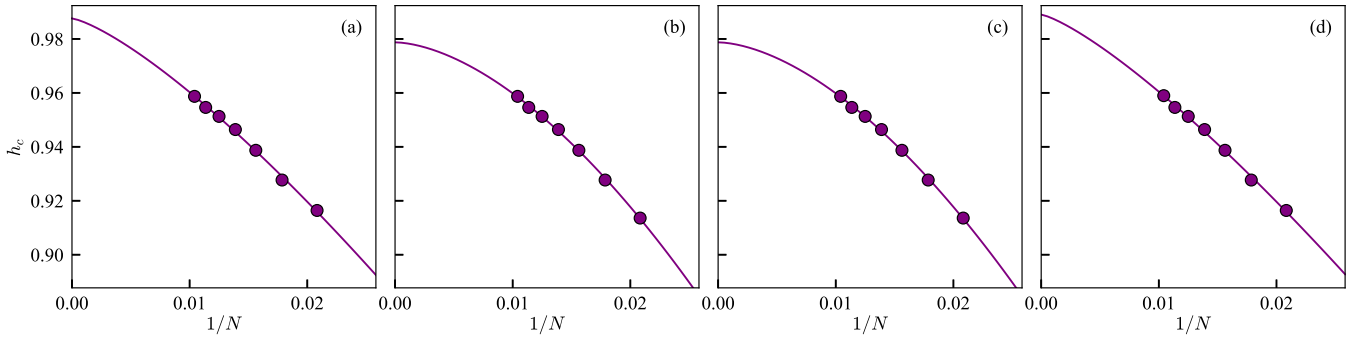

FIG. 9. Finite-size scaling of the pseudocritical point $h_c(N)$ as a function of inverse system size $1/N$ for (a) $\Delta = 0.0$, (b) $\Delta = 0.4$, (c) $\Delta = 0.6$, and (d) $\Delta = 0.8$. We use the polynomial fitting formula $h_c(N) = h_c^* + aN^{-1/\nu}$.

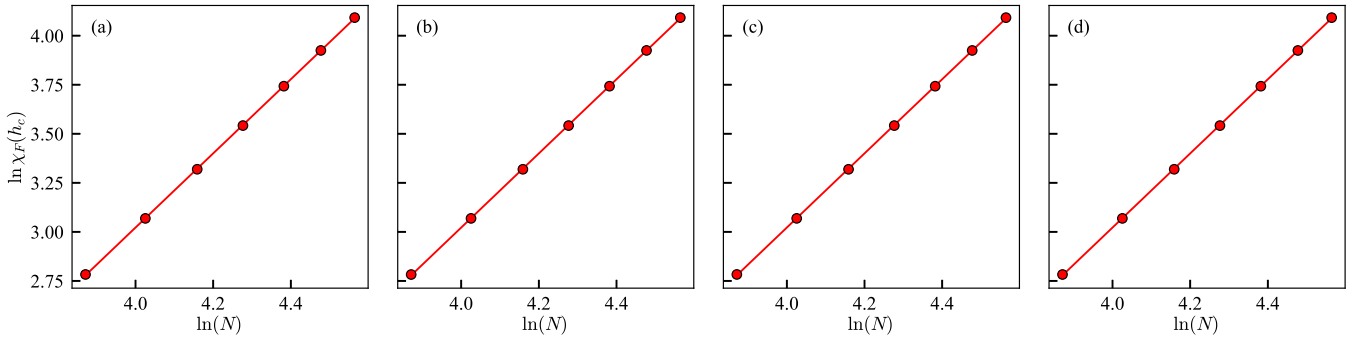

FIG. 10. Maximal fidelity susceptibility per site $\chi_F(h_c)$ as a function of system size N for (a) $\Delta = 0.0$, (b) $\Delta = 0.4$, (c) $\Delta = 0.6$, and (d)$\Delta = 0.8$ with $N = 48, 56, 64, 72, 80, 88, 96$ sites. We use the fitting formula $\chi_F(h_c) = N^{\mu}(c + dN^{-1})$.

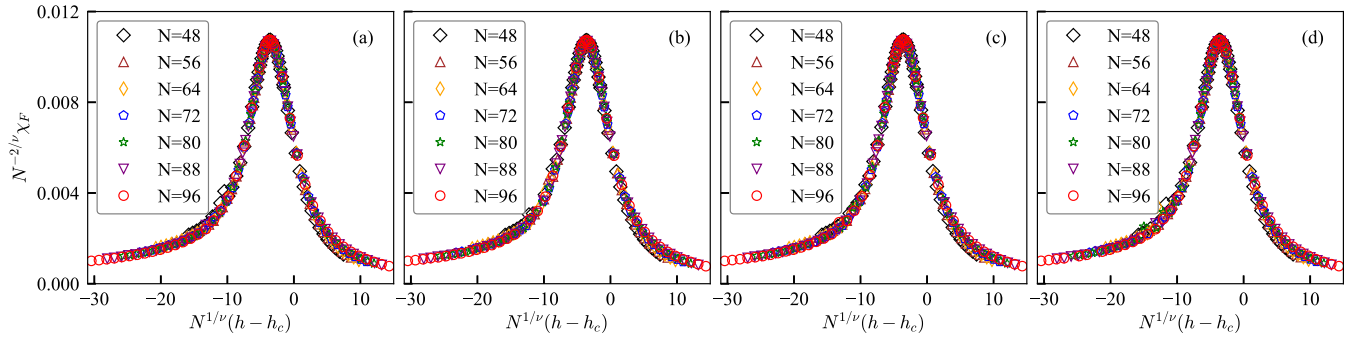

FIG. 11. Data collapse of fidelity susceptibility χ_F for the extended quantum XXZ spin chain for (a) $\Delta = 0.0$, (b) $\Delta = 0.4$, (c) $\Delta = 0.6$, and (d) $\Delta = 0.8$ with $N = 48, 56, 64, 72, 80, 88, 96$ sites as a function of the transverse field h.

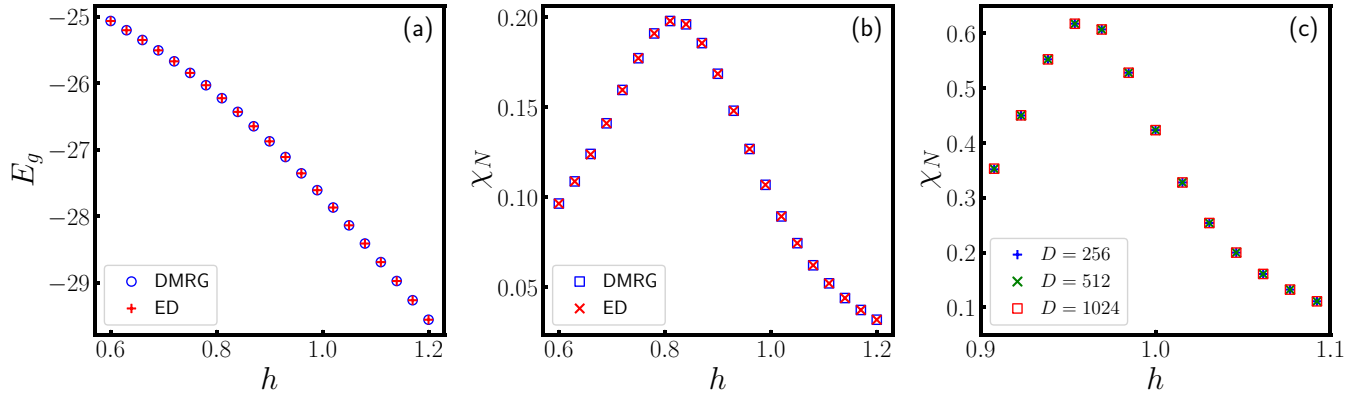

FIG. 12. Benchmarking against exact diagonalization for small system sizes. (a) Ground-state energy E_g and (b) fidelity susceptibility per site χ_N calculated separately by the DMRG method and exact diagonalization (based on the Lanczos algorithm) for system size $N = 24$ along the $\Delta = 0.4$ line. (c) Convergence of the fidelity susceptibility near the critical point for $N = 96$ along the $\Delta = 0.4$ line under OBC. The simulation is performed with MPS bond dimensions $D = 256$, 512, and 1024, respectively.

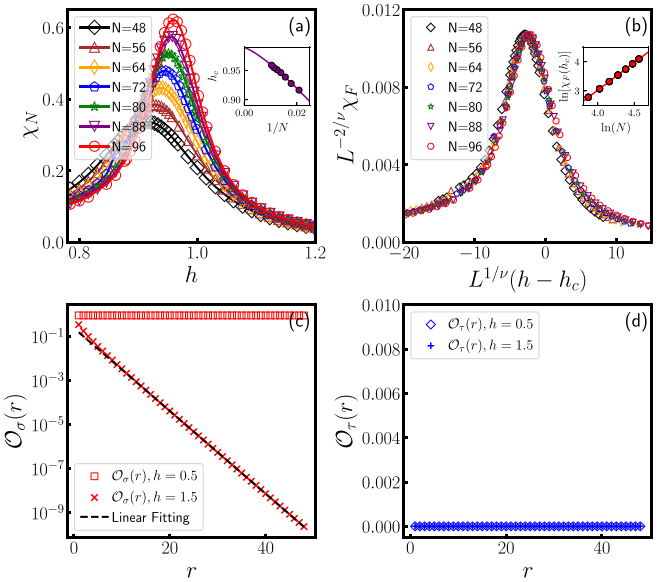

FIG. 13. (a) Fidelity susceptibility per site χ_N as a function of h for $\Delta = 2.0$ and $N = 48, 56, 64, 72, 80, 88, 96$. The inset exhibits the extrapolation of critical point h for the extended quantum XXZ spin chain. (b) Data collapse of fidelity susceptibility χ_F for the model for $\Delta = 2.0$, where $\nu \approx 1.058(3)$, $\mu \approx 1.890(5)$, and $h_c^* \approx 0.99(1)$ are used for data collapse plots. (c) and (d) Scaling behaviors of string correlations for $\Delta = 2.0$ with the simulated system size $N = 192$ under OBC.

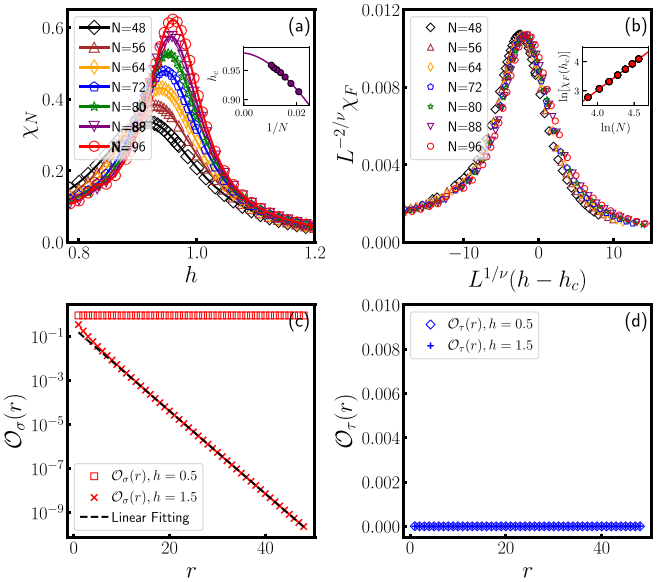

FIG. 14. (a) Fidelity susceptibility per site χ_N as a function of h for $\Delta = 3.0$ and $N = 48, 56, 64, 72, 80, 88, 96$. The inset exhibits the extrapolation of critical point h for the extended quantum XXZ spin chain. (b) Data collapse of fidelity susceptibility χ_F for the model for $\Delta = 3.0$, where $\nu \approx 1.058(3)$, $\mu \approx 1.890(5)$, and $h_c^* \approx 0.980(3)$. (c) and (d) Scaling behaviors of string correlations for $\Delta = 3.0$ with the simulated system size $N = 192$ under OBC.

also shows close alignment, confirming the robustness of the DMRG method results. In addition, the fidelity susceptibility is calculated with different MPS bond dimensions $D = 256$, 512, and 1024 for $\Delta = 0.4$ and $N = 96$ sites as shown in Fig. 12. It is clear that the bond dimension used in the work, namely, $D = 1024$, is sufficiently large to obtain converged and reliable results.

APPENDIX F: FIDELITY SUSCEPTIBILITY AND STRING CORRELATION FOR LARGE VALUES OF Δ

The model before the KT transformation is a quantum XXZ spin chain (τ spin) combined with an Ising symmetry-breaking Hamiltonian (σ spin) with a transverse field acting on even sites. In the large-Δ limit, by tuning the transverse field h, the ground state of the τ degrees of freedom corresponds to gapped spontaneous-symmetry-broken (SSB) phases, while the ground state of the σ degrees of freedom remains in the gapped SSB phase for $h < h_c$ and transitions to a trivial gapped phase for $h > h_c$. Therefore, after the KT transformation, the model no longer exhibits a phase transition between topologically distinct gapless phases. Instead, it displays a phase transition between distinct gapped phases, characterized by the Ising universality class due to $\mathbb{Z}_2$ symmetry breaking.

To numerically verify this physical understanding, in this Appendix we provide additional data showing the fidelity susceptibility and string correlations for large values of Δ. As shown in Figs. 13(a) and 14(a), we examined the fidelity susceptibility per site χ_N of the extended quantum XXZ spin chain for $\Delta = 2.0$ and 3.0 with $N = 48, 56, 64, 72, 80, 88, 96$ sites as a function of the transverse field h. The insets exhibit the extrapolation of the critical point h_c^* for the model. The data collapse of the fidelity susceptibility χ_F is presented for $\Delta = 2.0$ and 3.0 with $N = 48, 56, 64, 72, 80, 88, 96$ sites in Figs. 13(b) and 14(b), respectively. The insets show the finite-size scaling of the maximal fidelity susceptibility per site $\chi_N = \chi_F/N$ to obtain the correlation length exponent ν. The resulting critical points and exponents are also shown in Table I. The results demonstrate that a continuous phase transition exists at $h_c = 1$ even for $\Delta > 1.0$, with the correlation length exponent $\nu = 1$, consistent with the $(1+1)$-dimensional Ising universality class.

Additionally, we provide further data to identify possible quantum phases through the scaling behavior of string correlations for large values of $\Delta = 2.0$ and 3.0. Specifically, we compute the τ and σ string correlations as functions of lattice distance r to reveal the possible quantum phases, as depicted in Figs. 13(c), 13(d), 14(c) and 14(d). The results clearly show that the σ string exhibits long-range order below the critical point and exponential decay above it, while the τ string correlation is always zero since the gapless topological phases become topologically trivial gapped SSB phases for $\Delta > 1.0$.

[1] S. Sachdev, *Quantum Phase Transitions*, 2nd ed. (Cambridge University Press, Cambridge, 2011).

[2] S. Sachdev, *Quantum Phases of Matter* (Cambridge University Press, Cambridge, 2023).

[3] E. Fradkin, *Field Theories of Condensed Matter Physics* (Cambridge University Press, Cambridge, 2013).

[4] J. Cardy, *Scaling and Renormalization in Statistical Physics* (Cambridge University Press, Cambridge, 1996), Vol. 5.

[5] M. Z. Hasan and C. L. Kane, Colloquium: Topological insulators, Rev. Mod. Phys. **82**, 3045 (2010).

[6] X.-L. Qi and S.-C. Zhang, Topological insulators and superconductors, Rev. Mod. Phys. **83**, 1057 (2011).

[7] Z.-C. Gu and X.-G. Wen, Tensor-entanglement-filtering renormalization approach and symmetry-protected topological order, Phys. Rev. B **80**, 155131 (2009).

[8] X.-G. Wen, Colloquium: Zoo of quantum-topological phases of matter, Rev. Mod. Phys. **89**, 041004 (2017).

[9] T. Senthil, Symmetry-protected topological phases of quantum matter, Annu. Rev. Condens. Matter Phys. **6**, 299 (2015).

[10] X.-J. Yu, S.-H. Shi, L. Xu, and Z.-X. Li, Emergence of competing orders and possible quantum spin liquid in SU(n) fermions, Phys. Rev. Lett. **132**, 036704 (2024).

[11] X. Chen, Y.-M. Lu, and A. Vishwanath, Symmetry-protected topological phases from decorated domain walls, Nat. Commun. **5**, 3507 (2014).

[12] X. G. WEN, Topological orders in rigid states, Int. J. Mod. Phys. B **04**, 239 (1990).

[13] X. Chen, Z.-C. Gu, and X.-G. Wen, Complete classification of one-dimensional gapped quantum phases in interacting spin systems, Phys. Rev. B **84**, 235128 (2011).

[14] X. Chen, Z.-C. Gu, and X.-G. Wen, Local unitary transformation, long-range quantum entanglement, wave function renormalization, and topological order, Phys. Rev. B **82**, 155138 (2010).

[15] X. Chen, Z.-C. Gu, and X.-G. Wen, Classification of gapped symmetric phases in one-dimensional spin systems, Phys. Rev. B **83**, 035107 (2011).

[16] X.-G. Wen, Symmetry-protected topological invariants of symmetry-protected topological phases of interacting bosons and fermions, Phys. Rev. B **89**, 035147 (2014).

[17] X. Chen, Z.-C. Gu, Z.-X. Liu, and X.-G. Wen, Symmetry protected topological orders and the group cohomology of their symmetry group, Phys. Rev. B **87**, 155114 (2013).

[18] F. Pollmann and A. M. Turner, Detection of symmetry-protected topological phases in one dimension, Phys. Rev. B **86**, 125441 (2012).

[19] X.-G. Wen, Symmetry-protected topological phases in noninteracting fermion systems, Phys. Rev. B **85**, 085103 (2012).

[20] A. Keselman and E. Berg, Gapless symmetry-protected topological phase of fermions in one dimension, Phys. Rev. B **91**, 235309 (2015).

[21] M. Cheng and H.-H. Tu, Majorana edge states in interacting two-chain ladders of fermions, Phys. Rev. B **84**, 094503 (2011).

[22] L. Fidkowski, R. M. Lutchyn, C. Nayak, and M. P. A. Fisher, Majorana zero modes in one-dimensional quantum wires without long-ranged superconducting order, Phys. Rev. B **84**, 195436 (2011).

[23] J. P. Kestner, B. Wang, J. D. Sau, and S. Das Sarma, Prediction of a gapless topological Haldane liquid phase in a one-dimensional cold polar molecular lattice, Phys. Rev. B **83**, 174409 (2011).

[24] F. Iemini, L. Mazza, D. Rossini, R. Fazio, and S. Diehl, Localized Majorana-like modes in a number-conserving setting: An exactly solvable model, Phys. Rev. Lett. **115**, 156402 (2015).

[25] N. Lang and H. P. Büchler, Topological states in a microscopic model of interacting fermions, Phys. Rev. B **92**, 041118(R) (2015).

[26] T. Scaffidi, D. E. Parker, and R. Vasseur, Gapless symmetry-protected topological order, Phys. Rev. X **7**, 041048 (2017).

[27] J. Ruhman and E. Altman, Topological degeneracy and pairing in a one-dimensional gas of spinless fermions, Phys. Rev. B **96**, 085133 (2017).

[28] H.-C. Jiang, Z.-X. Li, A. Seidel, and D.-H. Lee, Symmetry protected topological Luttinger liquids and the phase transition between them, Sci. Bull. **63**, 753 (2018).

[29] R. Verresen, N. G. Jones, and F. Pollmann, Topology and edge modes in quantum critical chains, Phys. Rev. Lett. **120**, 057001 (2018).

[30] A. Keselman, E. Berg, and P. Azaria, From one-dimensional charge conserving superconductors to the gapless Haldane phase, Phys. Rev. B **98**, 214501 (2018).

[31] R. Verresen, Topology and edge states survive quantum criticality between topological insulators, arXiv:2003.05453.

[32] R. Verresen, R. Thorngren, N. G. Jones, and F. Pollmann, Gapless topological phases and symmetry-enriched quantum criticality, Phys. Rev. X **11**, 041059 (2021).

[33] C. M. Duque, H.-Y. Hu, Y.-Z. You, V. Khemani, R. Verresen, and R. Vasseur, Topological and symmetry-enriched random quantum critical points, Phys. Rev. B **103**, L100207 (2021).

[34] R. Thorngren, A. Vishwanath, and R. Verresen, Intrinsically gapless topological phases, Phys. Rev. B **104**, 075132 (2021).

[35] U. Borla, R. Verresen, J. Shah, and S. Moroz, Gauging the Kitaev chain, SciPost Phys. **10**, 148 (2021).

[36] X.-J. Yu, R.-Z. Huang, H.-H. Song, L. Xu, C. Ding, and L. Zhang, Conformal boundary conditions of symmetry-enriched quantum critical spin chains, Phys. Rev. Lett. **129**, 210601 (2022).

[37] D. E. Parker, T. Scaffidi, and R. Vasseur, Topological Luttinger liquids from decorated domain walls, Phys. Rev. B **97**, 165114 (2018).

[38] X.-J. Yu, S. Yang, H.-Q. Lin, and S.-K. Jian, Universal entanglement spectrum in gapless symmetry protected topological states, arXiv:2402.04042.

[39] X.-J. Yu and W.-L. Li, Quantum phase transition between topologically distinct quantum critical points, arXiv:2403.03716.

[40] W.-H. Zhong, W.-L. Li, Y.-C. Chen, and X.-J. Yu, Topological edge modes and phase transition in the critical fermionic chain with long-range interaction, arXiv:2403.11880.

[41] L. Li, M. Oshikawa, and Y. Zheng, Intrinsically/purely gapless-SPT from non-invertible duality transformations, arXiv:2307.04788.

[42] L. Li, M. Oshikawa, and Y. Zheng, Decorated defect construction of gapless-SPT states, arXiv:2204.03131.

[43] S.-J. Huang and M. Cheng, Topological holography, quantum criticality, and boundary states, arXiv:2310.16878.

[44] R. Wen and A. C. Potter, Bulk-boundary correspondence for intrinsically gapless symmetry-protected topological phases from group cohomology, Phys. Rev. B **107**, 245127 (2023).

[45] R. Wen and A. C. Potter, Classification of 1+1D gapless symmetry protected phases via topological holography, arXiv:2311.00050.

[46] S. Mondal, A. Agarwala, T. Mishra, and A. Prakash, Symmetry-enriched criticality in a coupled spin ladder, Phys. Rev. B **108**, 245135 (2023).

[47] L. Su and M. Zeng, Gapless symmetry-protected topological phases and generalized deconfined critical points from gauging a finite subgroup, Phys. Rev. B **109**, 245108 (2024).

[48] S. L. Sondhi, S. M. Girvin, J. P. Carini, and D. Shahar, Continuous quantum phase transitions, Rev. Mod. Phys. **69**, 315 (1997).

[49] X.-J. Yu, P.-L. Zhao, S.-K. Jian, and Z. Pan, Emergent spacetime supersymmetry at disordered quantum critical points, Phys. Rev. B **105**, 205140 (2022).

[50] L. D. Landau and E. M. Lifshitz, *Statistical Physics* (Elsevier, Amsterdam, 2013), Vol. 5.

[51] C. Xu, Unconventional quantum critical points, Int. J. Mod. Phys. B **26**, 1230007 (2012).

[52] T. Senthil, in *50 Years of the Renormalization Group: Dedicated to the Memory of Michael E. Fisher*, edited by A. Aharony, O. Entin-Wohlman, D. A. Huse, and L. Radzihovsky (World Scientific, Singapore, 2024).

[53] S. Yang, Z. Pan, D.-C. Lu, and X.-J. Yu, Emergent self-duality in a long-range critical spin chain: From deconfined criticality to first-order transition, Phys. Rev. B **108**, 245152 (2023).

[54] R. Verresen, R. Moessner, and F. Pollmann, One-dimensional symmetry protected topological phases and their transitions, Phys. Rev. B **96**, 165124 (2017).

[55] L. Tsui, H.-C. Jiang, Y.-M. Lu, and D.-H. Lee, Quantum phase transitions between a class of symmetry protected topological states, Nucl. Phys. B **896**, 330 (2015).

[56] L. Tsui, Y.-T. Huang, H.-C. Jiang, and D.-H. Lee, The phase transitions between $Z_n \times Z_n$ bosonic topological phases in $1+1$D, and a constraint on the central charge for the critical points between bosonic symmetry protected topological phases, Nucl. Phys. B **919**, 470 (2017).

[57] Y.-M. Lu and D.-H. Lee, Quantum phase transitions between bosonic symmetry-protected topological phases in two dimensions: Emergent QED_3 and anyon superfluid, Phys. Rev. B **89**, 195143 (2014).

[58] R. R. Kumar, N. Roy, Y. R. Kartik, S. Rahul, and S. Sarkar, Signatures of topological phase transition on a quantum critical line, Phys. Rev. B **107**, 205114 (2023).

[59] R. R. Kumar, Y. R. Kartik, and S. Sarkar, Topological phase transition between non-high symmetry critical phases and curvature function renormalization group, New J. Phys. **25**, 083027 (2023).

[60] Y. Yerin, C. Petrillo, and A. A. Varlamov, The Lifshitz nature of the transition between the gap and gapless states of a superconductor, SciPost Phys. Core **5**, 009 (2022).

[61] Y. Yerin, A. A. Varlamov, and C. Petrillo, Topological nature of the transition between the gap and the gapless superconducting states, Europhys. Lett. **138**, 16005 (2022).

[62] B. Hetényi, Interaction-driven polarization shift in the t-V-V' lattice fermion model at half filling: Emergent Haldane phase, Phys. Rev. Res. **2**, 023277 (2020).

[63] A. F. Albuquerque, F. Alet, C. Sire, and S. Capponi, Quantum critical scaling of fidelity susceptibility, Phys. Rev. B **81**, 064418 (2010).

[64] W. C. Yu, S.-J. Gu, and H.-Q. Lin, Fidelity susceptibilities in the one-dimensional extended Hubbard model, arXiv:1408.2642.

[65] D. Schwandt, F. Alet, and S. Capponi, Quantum Monte Carlo simulations of fidelity at magnetic quantum phase transitions, Phys. Rev. Lett. **103**, 170501 (2009).

[66] W.-C. Yu, H.-M. Kwok, J. Cao, and S.-J. Gu, Fidelity susceptibility in the two-dimensional transverse-field Ising and XXZ models, Phys. Rev. E **80**, 021108 (2009).

[67] G. Sun, A. K. Kolezhuk, and T. Vekua, Fidelity at Berezinskii-Kosterlitz-Thouless quantum phase transitions, Phys. Rev. B **91**, 014418 (2015).

[68] E. J. König, A. Levchenko, and N. Sedlmayr, Universal fidelity near quantum and topological phase transitions in finite one-dimensional systems, Phys. Rev. B **93**, 235160 (2016).

[69] B.-B. Wei, Fidelity susceptibility in one-dimensional disordered lattice models, Phys. Rev. A **99**, 042117 (2019).

[70] X.-J. Yu, S. Yang, J.-B. Xu, and L. Xu, Fidelity susceptibility as a diagnostic of the commensurate-incommensurate transition: A revisit of the programmable Rydberg chain, Phys. Rev. B **106**, 165124 (2022).

[71] Y.-T. Tu, I. Jang, P.-Y. Chang, and Y.-C. Tzeng, General properties of fidelity in non-Hermitian quantum systems with PT symmetry, Quantum **7**, 960 (2023).

[72] H.-L. Zhang, J.-H. Lv, K. Chen, X.-J. Yu, F. Wu, Z.-B. Yang, and S.-B. Zheng, Critical quantum geometric tensors of parametrically-driven nonlinear resonators, arXiv:2312.14414.

[73] X.-J. Yu, Dynamical phase transition and scaling in the chiral clock Potts chain, Phys. Rev. A **108**, 062215 (2023).

[74] X.-J. Yu, C. Ding, and L. Xu, Quantum criticality of a $\mathbb{Z}_3$-symmetric spin chain with long-range interactions, Phys. Rev. E **107**, 054122 (2023).

[75] Z.-X. Guo, X.-J. Yu, X.-D. Hu, and Z. Li, Emergent phase transitions in a cluster Ising model with dissipation, Phys. Rev. A **105**, 053311 (2022).

[76] G. Sun, B.-B. Wei, and S.-P. Kou, Fidelity as a probe for a deconfined quantum critical point, Phys. Rev. B **100**, 064427 (2019).

[77] G. Sun, J.-C. Tang, and S.-P. Kou, Biorthogonal quantum criticality in non-Hermitian many-body systems, Front. Phys. **17**, 33502 (2022).

[78] T. Kennedy and H. Tasaki, Hidden $Z_2 \times Z_2$ symmetry breaking in Haldane-gap antiferromagnets, Phys. Rev. B **45**, 304 (1992).

[79] M. Oshikawa, Hidden $Z_2 * Z_2$ symmetry in quantum spin chains with arbitrary integer spin, J. Phys.: Condens. Matter **4**, 7469 (1992).

[80] L. Li, M. Oshikawa, and Y. Zheng, Noninvertible duality transformation between symmetry-protected topological and spontaneous symmetry breaking phases, Phys. Rev. B **108**, 214429 (2023).

[81] P. Francesco, P. Mathieu, and D. Sénéchal, *Conformal Field Theory* (Springer Science+Business Media, New York, 2012).

[82] P. Ginsparg, in *Strings and Critical Phenomena*, edited by E. Brézin and J. Zinn Justin, Proceedings of the Les Houches Summer School of Theoretical Physics, XLIX, 1988 (North-Holland, Amsterdam, 1988).

[83] M. Levin and Z.-C. Gu, Braiding statistics approach to symmetry-protected topological phases, Phys. Rev. B **86**, 115109 (2012).

[84] S. R. White, Density matrix formulation for quantum renormalization groups, Phys. Rev. Lett. **69**, 2863 (1992).

[85] S. R. White, Density-matrix algorithms for quantum renormalization groups, Phys. Rev. B **48**, 10345 (1993).

[86] U. Schollwöck, The density-matrix renormalization group in the age of matrix product states, Ann. Phys. (NY) **326**, 96 (2011).

[87] U. Schollwöck, The density-matrix renormalization group, Rev. Mod. Phys. **77**, 259 (2005).

[88] G. Vidal, J. I. Latorre, E. Rico, and A. Kitaev, Entanglement in quantum critical phenomena, Phys. Rev. Lett. **90**, 227902 (2003).

[89] G. Vidal, Efficient classical simulation of slightly entangled quantum computations, Phys. Rev. Lett. **91**, 147902 (2003).

[90] G. Vidal, Efficient simulation of one-dimensional quantum many-body systems, Phys. Rev. Lett. **93**, 040502 (2004).

[91] F. Pollmann, A. M. Turner, E. Berg, and M. Oshikawa, Entanglement spectrum of a topological phase in one dimension, Phys. Rev. B **81**, 064439 (2010).

[92] T. V. Zache, C. Kokail, B. Sundar, and P. Zoller, Entanglement spectroscopy and probing the Li-Haldane conjecture in topological quantum matter, Quantum **6**, 702 (2022).

[93] A. W. Sandvik, in *Lectures on the Physics of Strongly Correlated Systems XIV: Fourteenth Training Course in the Physics of Strongly Correlated Systems, Vietri sul Mare, 2009*, edited by A. Avella and F. Mancini, AIP Conf. Proc. No. 1297 (American Institute of Physics, Melville, 2010), pp. 135–338.

[94] M. Fishman, S. R. White, and E. M. Stoudenmire, The ITensor software library for tensor network calculations, SciPost Phys. Codebases **4**, 1 (2022).